JACC: CARDIOVASCULAR IMAGING
VOL. 9, NO. 7, 2016
© 2016 BY THE AMERICAN COLLEGE OF CARDIOLOGY FOUNDATION
ISSN 1936-878X/$36.00
PUBLISHED BY ELSEVIER
http://dx.doi.org/10.1016/j.jcmg.2016.03.009

Multimodality Imaging for Guiding EP Ablation Procedures

Mario Njeim, MD,[a] Benoit Desjardins, MD, PhD,[b] Frank Bogun, MD[a]

ABSTRACT

Recent advances in 3-dimensional electroanatomical mapping have been met by continuous improvements in the field of cardiac imaging and image integration during ablation procedures. Echocardiography, computed tomography, cardiac magnetic resonance, and nuclear imaging provide information about cardiac anatomy and ultrastructure of the heart that may be crucial for a successful ablation procedure. Techniques and value of pre-procedural, intraprocedural, and post-procedural imaging and image integration are discussed in this review article. Pre-procedural imaging provides key anatomic information that can be complemented by intraprocedural imaging to minimize procedural complications. Furthermore, the presence and extent of structural heart disease can be assessed pre-procedurally and can be displayed intraprocedurally to limit and focus the mapping and ablation procedure to the area of interest. Pre-procedural imaging combined with imaging obtained during the ablation procedure further enhances procedural safety, reduces exposure to ionizing radiation from fluoroscopy, reduces procedure time, and may improve outcomes. (J Am Coll Cardiol Img 2016;9:873–86) © 2016 by the American College of Cardiology Foundation.

Over the last several decades, imaging has become an integral part of electrophysiological procedures. Integration of various imaging modalities like echocardiography, cardiac magnetic resonance (CMR), computed tomography (CT), and nuclear imaging have contributed to further advances in the field of electrophysiology.

The trend of image integration in electrophysiology has been strengthened by the realization that the anatomic structure and ultrastructure of the heart play key roles in arrhythmogenesis. Precise representation of a catheter tip equipped with a localizing sensor is the key element of the 3-dimensional (3D) electroanatomical mapping systems that are currently used for ablation procedures in complex ventricular and atrial arrhythmias. A common platform of the electroanatomical mapping system with several imaging modalities allows data of CT, CMR, and echocardiographic imaging to be integrated into the electroanatomical mapping systems used for ablation. More and more electrophysiologists world wide use imaging data to assist with electrophysiology procedures (1). This overview discusses the use and benefit of multimodality imaging techniques during atrial and ventricular ablation procedures, including pre-procedural, intraprocedural, and post-procedural imaging (Table 1).

ELECTROANATOMICAL MAPPING FOR ABLATION PROCEDURES

3D reconstruction of the cardiac anatomy combined with electrophysiological information is the basis for mapping and ablation of complex atrial and ventricular arrhythmias (Central Illustration). Precise identification of a catheter tip in 3D space combined with acquisition of essential information about tissue integrity (Figure 1) have largely improved the ability to navigate catheters within the cardiac chambers to areas of interest (2,3). Several mapping systems exist. The 2 most commonly used 3D electroanatomical mapping systems are the Carto system (Biosense Webster, Diamond Bar, California), which is based on a magnetic sensor, and NavX Ensite (St. Jude Medical, St. Paul, Minnesota), an impedance-based 3D mapping system. The Carto system is a nonfluoroscopic system that uses magnetic technology to determine catheter location in 3D space. A magnetic field is generated from an emitter consisting of 3 coils that is mounted under the operating table. A sensor

From the [a]Division of Cardiovascular Medicine, University of Michigan, Ann Arbor, Michigan; and the [b]Department of Radiology, University of Pennsylvania, Philadelphia, Pennsylvania. Dr. Bogun has received research support from Biosense Webster. All other authors have reported that they have no relationships relevant to the contents of this paper to disclose.

Manuscript received December 21, 2015; revised manuscript received February 22, 2016, accepted March 10, 2016.

ABBREVIATIONS AND ACRONYMS

ARVD = arrhythmogenic right ventricular dysplasia

CMR = cardiac magnetic resonance

CT = computed tomography

ICE = intracardiac echocardiography

MIBG = metaiodobenzylguanidine

SPECT = single-photon emission computed tomography

TEE = transesophageal echocardiography

VT = ventricular tachycardia

embedded within the catheter tip allows for 3D localization of the tip by detecting the intensity of the magnetic field. The NavX system technology uses an electrical field generated between external patches placed along 3 orthogonal axes on the patient. As a catheter is moved within the electrical field, the different electrodes sense the impedance that is derived from the measured voltage between the different axes and thereby determine the 3D location of the catheter electrodes within the electrical field. Both of the 3D mapping systems are used to map the cardiac chambers and allow for 3D reconstruction of the mapped chambers (2,4). Electroanatomical mapping helps to minimize exposure to ionizing radiation by minimizing fluoroscopy (5-7), which is used conventionally to guide catheter manipulation.

ELECTROANATOMICAL MAPS AND IMAGING

Both of the electroanatomical mapping systems allow for integration of data derived from CT or CMR into the electroanatomical maps, thereby providing additional information that may result in improved efficacy and increased safety of ablation procedures. The ensuing registration error is similar in both of the systems. A randomized study comparing both systems in patients undergoing ablation procedures for atrial fibrillation concluded that use of the Carto system resulted in faster and more reliable image integration than NavX and that, therefore, less fluoroscopy may be necessary. However outcomes were similar in both of the patient groups (8). No other randomized comparisons between both systems have been reported, and a trial aimed to compare both systems was terminated early due to lack of enrolment. Other differences include the fact that, in the Carto system, visualization of catheters is limited to ablation catheters manufactured by Biosense Webster. Both of the systems have a high spatial resolution for catheter position (range 1 mm) and use algorithms to compensate for cardiac shifts related to respiratory motion. NavX defines the map surface using the most distant points from a geometric center. This algorithm leads to chamber oversizing secondary to protrusion of the mapping catheter against the cardiac wall and also to anatomical distortions. There are many other mapping systems, including Rhythmia (Charlestown, Massachusetts), Topera (Palo Alto, California), noncontact mapping, and CardioInsight (Cleveland, Ohio), to name a few. Discussing these systems is beyond the scope of this review article that focuses on how imaging techniques can facilitate ablation procedures.

Image integration aims to achieve 4 major objectives: 1) minimize the radiation exposure to patient and health care providers; 2) enhance procedural outcomes; 3) shorten procedure times; and 4) minimize the potential for procedure-related complications. These points are highlighted in this review.

TABLE 1 Benefit of Imaging Depending on Type of Ablation Procedure

Procedure	Imaging Benefit
Ablation for atrial fibrillation	
Paroxysmal AF	CT/CMR for PV anatomy*(75-77)
Persistent/chronic AF	
Ablation of post MI VT	CMR for scar location†
Ablation of VT in NICM	
Endocardial ablation	CMR for scar location†
Epicardial ablation	Cardiac CT for coronary artery and phrenic nerve location†
Ablation of idiopathic VA	
Ablation of PAP VA	Intracardiac echo†
Ablation of cusp VA	Intracardiac echo†
Ablation of other idiopathic VA	Intracardiac echo* (78)

*Demonstrated benefit is reduction in fluoroscopy and/or procedure time. †Clear benefit not demonstrated.

AF = atrial fibrillation; CMR = cardiac magnetic resonance; echo = echocardiography; MI = myocardial infarction; NICM = nonischemic cardiomyopathy; PAP = papillary muscle; PVI = pulmonary vein isolation; VA = ventricular arrhythmia; VT = ventricular tachycardia.

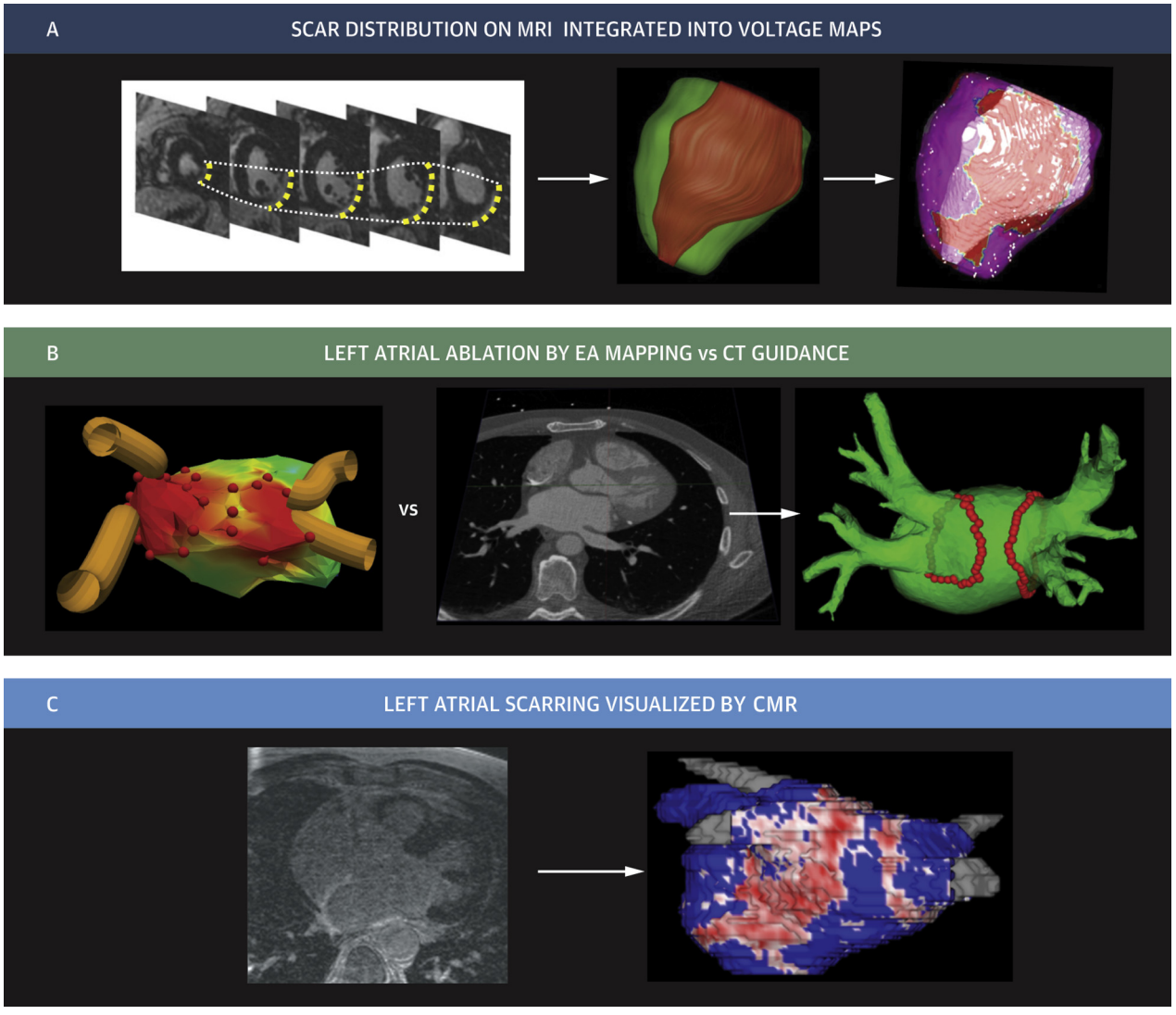
IMAGING FOR ATRIAL ABLATION PROCEDURES

PRE-PROCEDURAL IMAGING AND IMAGE INTEGRATION. Pre-procedural atrial imaging focuses on determining atrial anatomy, scarring, and adjacent structures. The information provided can be used for: 1) defining the atrial anatomy and adjacent structures; 2) ruling out atrial thrombi; 3) assessing the degree of atrial scarring; and 4) identification of anatomic landmark structures used for intraprocedural image registration into the electroanatomical map.

Knowledge of patient-specific anatomy (9,10) of the pulmonary veins facilitates guiding catheter manipulation and delivery of radiofrequency energy at antral or ostial locations, thereby reducing the risk of pulmonary vein stenosis. Furthermore, the right pericardiophrenic artery can be visualized by CT, which helps to reliably locate the right phrenic nerve (**Figure 2**) (11). Such a technique has been shown to identify patients more vulnerable to phrenic nerve injury during balloon-based ablation procedures (10).

Recently, a multicenter retrospective analysis in patients with paroxysmal atrial fibrillation undergoing circumferential pulmonary vein isolation showed

CENTRAL ILLUSTRATION **Electroanatomic Mapping, Ablation, and Imaging**



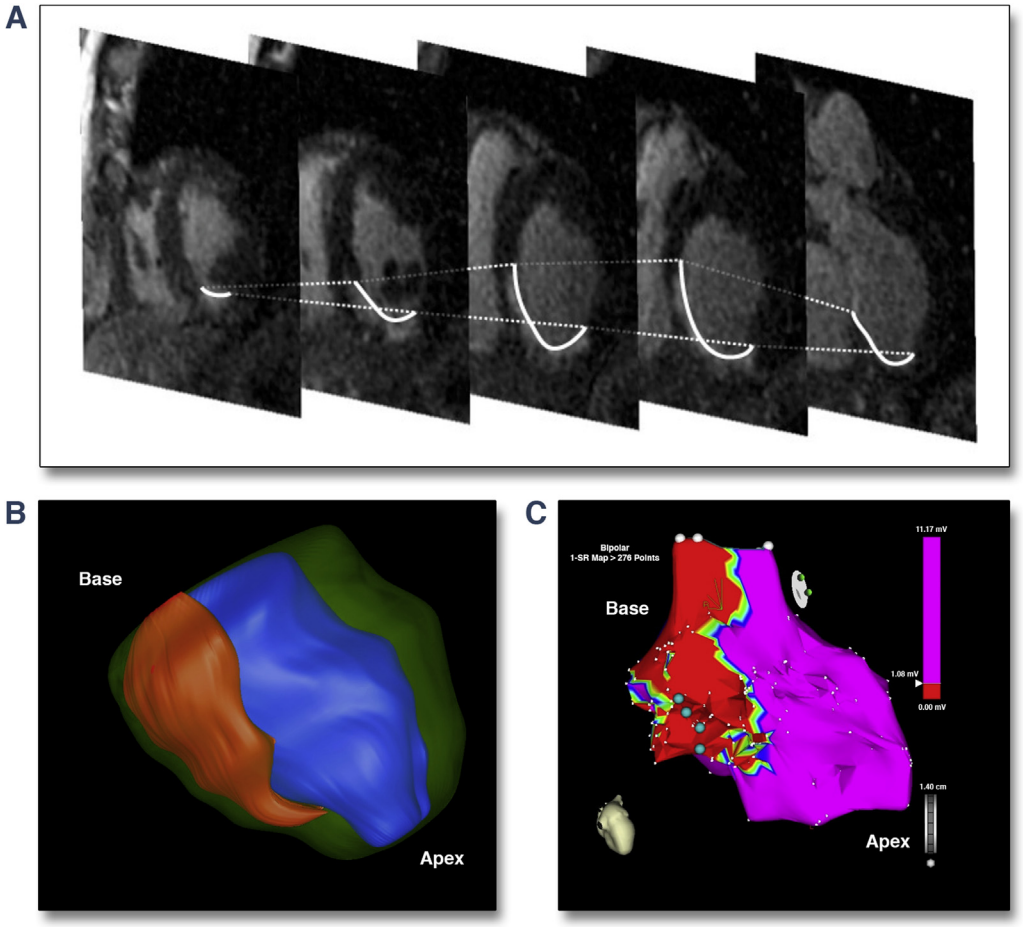
Njeim, M. et al. J Am Coll Cardiol Img. 2016;9(7):873–86.

(A) Shown is the display of an epicardial scar on a stack of short axis cardiac magnetic resonance (CMR) images; the scar is shown as a 3-dimensional (3D) reconstruction in the **middle panel** and in the **left panel** the scar is integrated in the electroanatomic voltage map. **(B)** Electroanatomic reconstruction of the left atrium with the pulmonary veins; **middle panel** indicates a computed tomography (CT) view of the left atrium and the **panel on the right** illustrates a CT based 3D reconstruction of the left atrium with the pulmonary veins that is used during circumferential ablation of the pulmonary vein antrum. **(C)** Scar in the left atrium shown in CMR **(left panel)**, 3D reconstruction of the scar within the left atrium.

significant improvement in freedom from atrial arrhythmias when image integration was used in comparison with both 3D mapping and segmental electrophysiology-guided pulmonary vein isolation (12). Randomized studies thus far, however, have failed to demonstrate a superior outcome when imaging was used.

Pre-procedural imaging has important limitations compared to real-time imaging. Esophageal imaging in order to avoid ablation-induced atrioesophageal fistulas represents one of these limitations. Although the esophagus can be delineated using CT or CMR imaging (13), the esophagus is a mobile structure, and it can shift sideways by ≥2 cm in patients

FIGURE 1 Late Gadolinium Enhancement CMR in Prior Myocardial Infarction



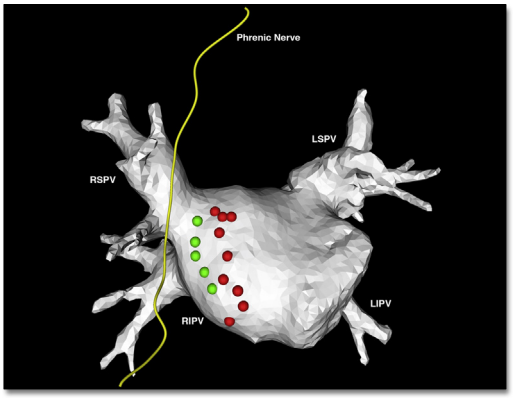
(A) Stack of short-axis CMR images with delayed gadolinium enhancement (DE) in the inferoseptal left ventricle. The subendocardial area of DE is pointed out by the **white contour** lines. **(B)** 3D reconstruction of the subendocardial scar as shown in the CMR image. The scar is **orange**, the LV endocardium is indicated in **blue**, and the epicardium is **green**. **(C)** Electroanatomical voltage map (bipolar) of a view similar to that in **B**. Scar is indicated in **red**, and normal tissue is shown in **purple**. Four **light blue tags** indicate critical sites for VT in this patient. CMR = cardiac magnetic resonance; DE = delayed enhancement; LV = left ventricular; VT = ventricular tachycardia.

undergoing catheter ablation for atrial fibrillation under conscious sedation (14). Therefore, real-time esophageal imaging is preferable.

LEFT ATRIAL THROMBI. Transesophageal echocardiography (TEE) is the modality most commonly used to rule out left atrial thrombi prior to atrial fibrillation ablation procedures. Intracardiac echocardiography in the pulmonary artery position has also been used intraprocedurally for the detection of thrombi, and has been reported to be comparable or even better than TEE in patients undergoing catheter ablation procedures (15). Alternative imaging modalities including CT and CMR have also been used to screen for left atrial thrombi (16,17).

ATRIAL VOLUME AND FIBROSIS. Left atrial volume and left atrial fibrosis have been used as predictors of outcomes of atrial fibrillation ablation. Left atrial dimensions as assessed by echocardiography and CT showed an incremental predictive value of the left atrial volume over left atrial diameters, as well as the advantage of CT over echocardiography (18). Degree and extent of scarring as assessed with late gadolinium enhancement in CMR has been found to predict the rate of recurrence of atrial fibrillation following

FIGURE 2 CT Illustrates the 3D Path of the Right Phrenic Nerve With Respect to the Left Atrium Imported Into the Electroanatomical Map

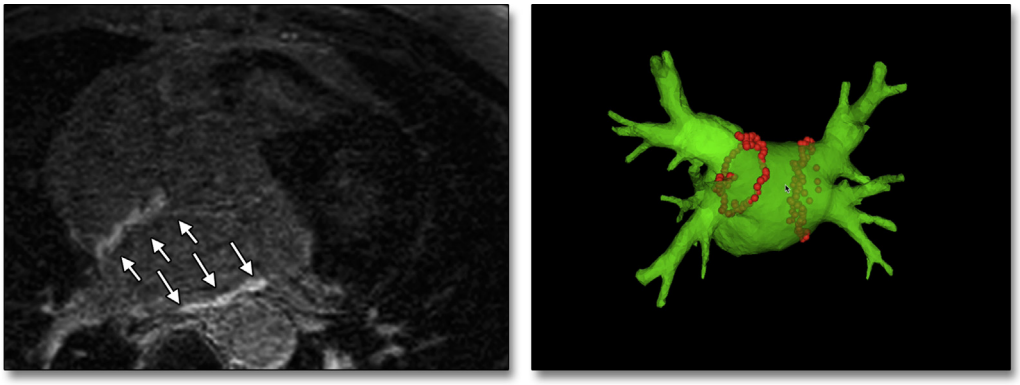


Focal electrical stimuli at the surface of the left atrium show capture **(green)** or noncapture **(red)** of the right phrenic nerve. The left atrial appendage is not displayed. Pulmonary veins are indicated. CT = computed tomography; LIPV = left inferior pulmonary vein; LSPV = left superior pulmonary vein; RIPV = right inferior pulmonary vein; RSPV = right superior pulmonary vein; 3D = 3-dimensional.

catheter ablation (19), independently of the type of atrial fibrillation and associated comorbidities (20). It is conceivable that such a prognostic tool might help to select appropriate candidates for atrial fibrillation ablation. The limited reproducibility and technical difficulties in imaging, displaying, and quantifying atrial fibrosis in different centers at present is the major limitation of this imaging modality.

INTRAPROCEDURAL IMAGING: REAL-TIME INTRACARDIAC ECHOCARDIOGRAPHY. Intracardiac echocardiography (ICE) is beneficial when used in combination with atrial and ventricular ablation procedures. The phased array system uses a 64-element vector-phased array (AcuNav, Acuson, Siemens, Erlangen, Germany). The catheter probe is steerable, has tissue penetration up to 16 cm, variable ultrasound frequency, and Doppler capability. Furthermore, it can be integrated into an electroanatomical mapping system (e.g., CartoSound, Biosense Webster). In the atrium, the ultrasound probe is used mainly from within the right atrium. It is used to guide and facilitate transseptal puncture, visualize pulmonary vein ostia, and identify other potential ablation targets. The esophagus can also be visualized and marked to avoid collateral damage (21). ICE does allow for 3D reconstructions of the left atrium that can be accomplished during the ablation procedure, offering the advantage of nearly real-time imaging during the ablation procedure, which enables navigation within the left atrium in order to minimize radiation exposure to patient and operator. Furthermore, ICE helps to recognize complications (22) like perforations that result in pericardial effusions, early, before the actual

FIGURE 3 Left Atrial Ablation Lesions



(Left) Late gadolinium enhancement CMR after left atrial ablation therapy **(white arrows)**. Areas of ablation show as high-intensity lesions in the interatrial septum and posterior wall of the left atrium, anterior to the descending thoracic aorta. **(Right)** Left atrial and pulmonary vein 3D anatomy as assessed by CT, incorporated into the electroanatomical map, is used to guide placement of the ablation lesions in real time (same orientation as in Figure 2). Linear lesions without gaps around the ostia of the pulmonary veins are generated by a series of collinear punctiform lesions, to electrically isolate the pulmonary veins from the remaining of the left atrium. Abbreviations as in Figures 1 and 2.

development of cardiac tamponade and, therefore, allows for an early intervention to further contain complications.

POST-PROCEDURAL IMAGING. Post-procedural imaging with late gadolinium-enhanced CMR has been used to assess reasons for atrial fibrillation recurrences (**Figure 3**) (23,24). The presence of gaps in ablation lines has been implicated as one of the reasons for atrial fibrillation recurrence. Also, the absence of ablation lesions in areas where radiofrequency energy was thought to have been delivered points to inadequate contact being responsible for atrial fibrillation recurrence (25). Intraprocedural assessment of lesion formation may be helpful in avoiding this issue. Good contact between the mapping catheter and the myocardial wall is critically important to generate a lesion within the myocardium aimed at eliminating atrial or ventricular arrhythmias. For atrial arrhythmias, the ablation strategy often involves deployment of linear lesions using a series of adjacent punctiform lesions in order to achieve pulmonary vein isolation, and it is crucial that the punctiform lesions are confluent without any gaps. Gaps can result in pulmonary vein reconnection and recurrence of atrial fibrillation, or in resurgence of atypical atrial flutter. Conventionally, impedance and echocardiography have been used as ancillary methods to confirm that a catheter is in good contact with the myocardial wall. Further improvement in catheter technology reflects the level of contact force exerted by the catheter on the myocardium and thereby may reduce to some degree the need of imaging for this purpose. Several recent clinical studies have suggested that contact force sensing can improve clinical outcomes, shorten fluoroscopy times, and reduce the risk of cardiac perforation during radiofrequency ablation for atrial fibrillation procedures (26,27).

Lesion formation has been assessed with echocardiography and CMR. Dickfeld et al. (28) investigated the time course of contrast enhancement of radiofrequency energy lesions. The different phases are similar to the phases of enhancement seen with myocardial infarction. The wash-in and washout kinetics, however, are quite different for radiofrequency energy lesions. The timing to completely enhance with gadolinium takes approximately 1.5 h for radiofrequency lesions, compared to 10 min for post-infarction tissue (29). It is thought that more severe tissue necrosis is responsible for the altered wash-in kinetics of radiofrequency lesions. The late contrast up-take is problematic if gadolinium is used for real-time imaging of lesion formation. More recently, noncontrast T_1 imaging has been described for acutely visualizing the core lesion and the surrounding edema (30). The distinction between edema and core of an ablation lesion is critical if the objective is to create permanent linear lesions without interrupting gaps because gaps in these lesions as assessed by CMR have been correlated with recurrence after atrial fibrillation ablation procedures (31,32). An alternative imaging modality for ablation lesions is acoustic radiation force imaging that images tissue elasticity by delivering impulses to the myocardium, resulting in mechanically displacing tissue (33). The magnitude of tissue displacement or elasticity indicates the location of lesions (i.e., stiffer tissue indicates ablation lesions, whereas areas with more elasticity indicate nonablated tissue and therefore can indicate gaps within an ablation lesion). Currently no method is routinely used to assure that permanent lesions were actually delivered to an area of interest. Efforts to ensure that ablation lesion delivery results in permanent contiguous lesions are the subject of ongoing research.

IMAGING FOR VENTRICULAR ABLATION PROCEDURES

PRE-PROCEDURAL IMAGING: CMR. Eletroanatomical mapping is key for targeting complex ventricular arrhythmias. Voltage mapping data obtained during the mapping procedure are displayed in the form of a voltage map (bipolar or unipolar) and reflect the location of scar tissue (**Figure 1**) (34). Validation studies have confirmed that low endocardial voltage (bipolar voltage <1.5 mV) corresponds to the presence of scar tissue as defined by late gadolinium-enhanced CMR (35–37). It has been demonstrated that myocardial scar contains most of the arrhythmogenic substrate in patients with prior myocardial infarction (**Figure 1**) and other forms of cardiomyopathy (36,38). Scar distribution depends on the underlying cardiomyopathy, and the information about location and extent of scarring can be used to plan an ablation procedure.

IMAGING OF THE ARRHYTHMOGENIC SUBSTRATE IN STRUCTURAL HEART DISEASE. Late gadolinium enhancement after intravenous administration of gadolinium is the gold standard for detecting myocardial scar tissue (29,39).

Pre-procedural CMRs have been extremely helpful in localizing scar tissue in the ventricles and have helped to guide and target the arrhythmogenic tissue (38,40,41) with catheter ablation. However, although some reports have found good correlation between areas of low bipolar voltage and CMR-defined scarring (36), others have reported discrepancies between

voltage maps and extent of scarring in CMR (37). Lack of contact between the mapping catheter and the myocardial wall results in an erroneously low voltage as well as an incomplete sampling, allowing the mapping system to extrapolate data points from mapped areas to areas that actually have not been mapped. This may be a reason for the discrepancy between scar tissue observed in a CMR and that on an electroanatomical voltage map. Integration of the scarring into the electroanatomical map can be accomplished while the electroanatomical map is constructed, thereby focusing on an area of interest (42). Although the information of scar location in post-infarction patients helps to guide the ablation catheter to a region of interest, the structure that is critical for reentrant ventricular tachycardia (VT) (i.e., myofiber bundles embedded in scar tissue) is beyond the imaging resolution of current clinical CMRs. More recently, differences in signal intensities within scar tissue have been correlated with "channels" in the electroanatomical voltage maps of post-infarction patients and have been found to indicate critical areas for post-infarction VT within the scar tissue (43). Lower signal intensities within scar tissue are thought to indicate surviving muscle bundles within dense scar tissue. This technique, however, has not yet prevailed, and other studies were unable to demonstrate differences in signal intensity at sites critical for post-infarction VT compared to other sites within the scar (36). Many patients with VT have cardiac-implanted electronic devices and therefore may not be able to undergo CMRs at all institutions. Wall thinning and/or hypoperfusion as assessed with cardiac CT has been found to indicate scar tissue (44). Therefore CT can be used as an alternative to CMR to assess for scarring if CMRs cannot be obtained. Unipolar voltage mapping (45,46) also has been used as an alternative to CMR to assess for deeper seated scar tissue. The wide range of overlap with normal tissue, however, makes this method less precise.

Post-infarction scarring is associated with sympathetic denervation. This can be assessed qualitatively with single-photon emission CT (SPECT) imaging with the use of iodine-123-labeled metiaodobenzylguanidine ([^{123}I]MIBG). The denervation defect is usually larger than the size of scarring in post-infarction patients (47,48). It has been demonstrated that viable but denervated myocardium is particularly sensitive to development of arrhythmias (49,50). Klein et al. (51) were able to integrate [^{123}I]MIBG data within the electroanatomical maps and demonstrated that all critical VT ablation sites were located in denervated areas, some of which were located in areas with preserved bipolar voltage. The underlying mechanism of arrhythmia from this denervated arrhythmogenic substrate is not clear, however. Further investigation of the impact of sympathetic denervation and its potential value to guide ablation procedures would require a higher spatial resolution than SPECT as well as a superior quantification over [^{123}I]MIBG studies. Positron emission tomography offers both of these features, and imaging with [^{11}C]meta-hydroxyephedrine may be superior to that with [^{123}I]MIBG imaging for this objective (52).

In patients with nonischemic cardiomyopathy, scar tissue is predominantly intramurally located (53); epicardial or endocardial scarring is less frequent. In these patients, one of the most important questions prior to the ablation procedure is whether an epicardial subxiphoid procedure (54), which is more invasive and prone to complications than an endocardial approach, is necessary. Pre-procedural imaging with CMR is helpful in this regard. The location of scarring as determined by CMR has been correlated with the planning and outcomes of ablation procedures (38). If the scar was mainly endocardial, all arrhythmias could be eliminated endocardially; if there was predominantly epicardial scarring, all arrhythmias could be ablated epicardially; on the other hand, ablations failed for intramural arrhythmias. More recently, with respect to intramural scars, pre-procedural CMRs were used prospectively to target VTs in patients with failed VT ablation procedures (40). Intramural scar located in the left ventricular free wall was approached endocardially and epicardially, whereas intramural scar in the septum was approached through the left and right ventricular endocardium. VTs were eliminated in most patients using this approach.

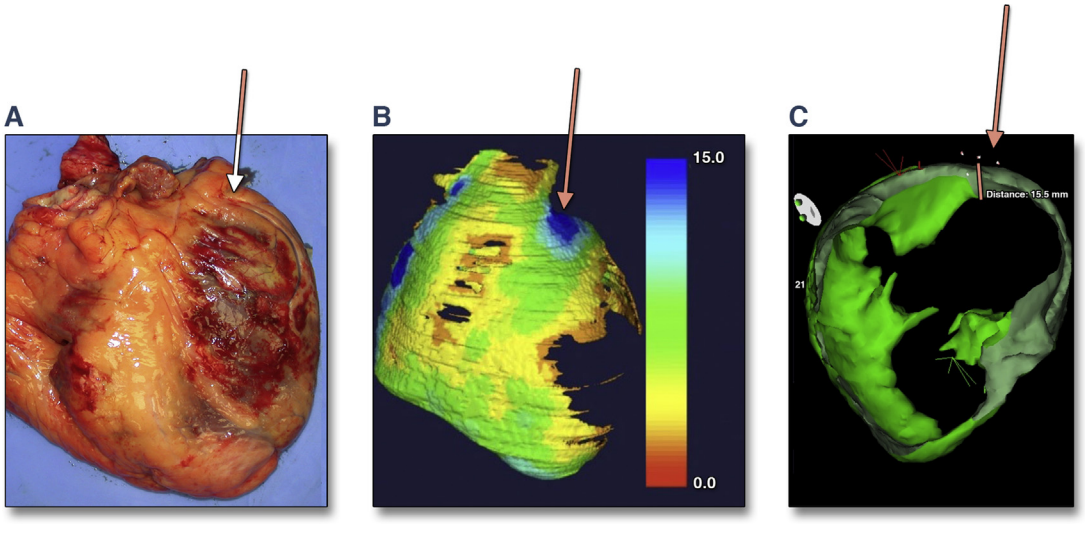
CMR and CT imaging are used mainly for their diagnostic value in patients with arrhythmogenic right ventricular dysplasia (ARVD) (55). CT-derived fat imaging data were correlated with the arrhythmogenic substrate in a small series of patients with ARVD (56). A few case series exist in patients with hypertrophic cardiomyopathy, where ablation of VT was performed (57,58); however, in none of these reports was a systematic image-guided ablation approach used.

Epicardial mapping and ablation procedures are frequently carried out in patients with nonischemic cardiomyopathies. Multimodality imaging is particularly beneficial for these procedures to avoid collateral damage. In the presence of epicardial fat, the bipolar amplitude of epicardial electrocardiograms is attenuated, depending on the thickness of epicardial fat (59), as detected by CT (**Figure 4**). Therefore, voltage mapping with the ablation

catheter alone is not sufficient to detect scar tissue. The combination of low voltage and fragmented electrocardiograms is required in the epicardium for identification of scar tissue. Ablation procedures over a layer of epicardial fat >10 mm failed to eliminate epicardial arrhythmias (59). This information is particularly relevant for patients with idiopathic epicardial ventricular arrhythmias that often originate from the basal aspect of the left ventricle, which is often sheltered under a thick layer of epicardial fat tissue, resulting in a low success rate for eliminating these types of arrhythmias with the percutaneous subxiphoid approach (60,61). Using CT angiograms, Carriagan et al. (60) carefully measured the distance from the coronary venous system to the epicardial myocardium and compared it to the distance from the pericardial space to the basal left ventricular epicardial myocardium. The distance was significantly less from the coronary venous system than from the pericardial space (60), a fact that is reflected by the higher success rate of ablation from within the coronary venous system and adjacent structures (62,63) than ablations from within the pericardial space. Epicardial fat is not the only reason for the inability to eliminate epicardial ventricular arrhythmias. Coronary arteries are embedded in epicardial fat, and delivery of radiofrequency energy adjacent to the arteries has resulted in damage to the coronary arteries in animal studies (64). Different strategies have been used to avoid this scenario, including obtaining coronary angiograms prior to delivery of radiofrequency energy or visualization of the coronary vessels from CT angiograms that are imported into the mapping procedure (**Figure 5**). Once the coronary arteries have been visualized, maintaining a distance of 5 to 10 mm between ablation lesions and the closest coronary artery is prudent to avoid vascular damage. The phrenic nerve can also be damaged during epicardial ablation procedures. It can be identified by high-output pacing, resulting in diaphragmatic stimulation or by direct preprocedural visualization of the phrenic nerve (**Figures 2 and 5**) (65). If a critical location for VT is adjacent to the phrenic nerve, different measures have been described to mechanically separate the parietal pericardium from the epicardial myocardium by the use of a balloon or fluid (66,67) in order to avoid damage to the phrenic nerve, which runs along the parietal pericardium.

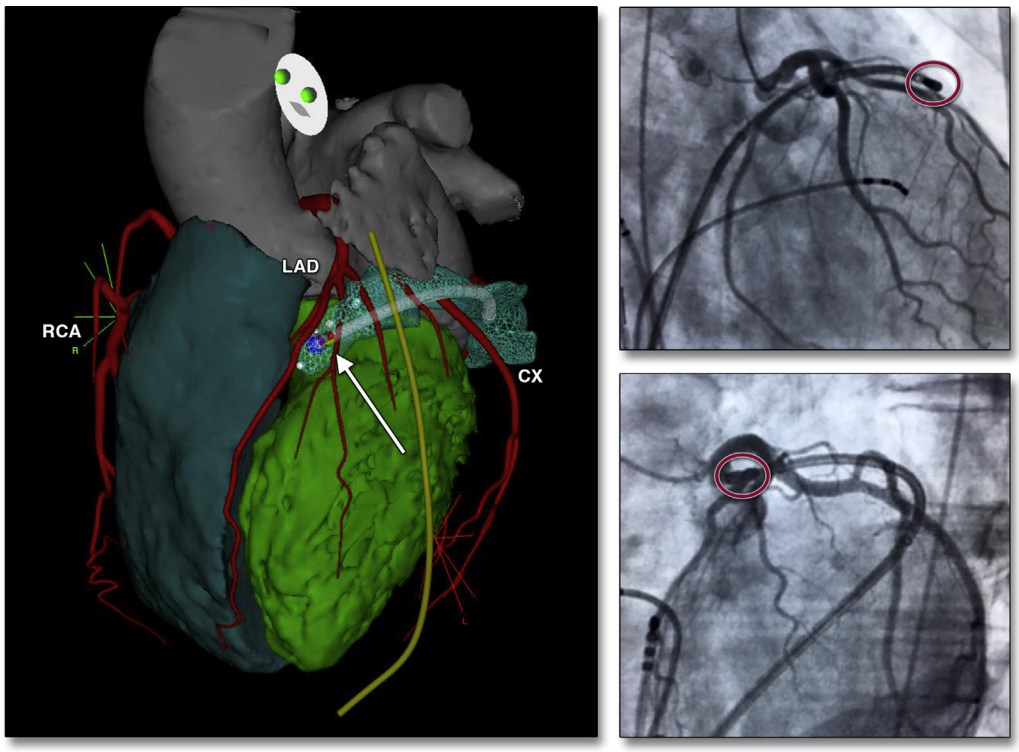
INTRAPROCEDURAL IMAGING DURING VT ABLATION PROCEDURES. Similar to intraprocedural imaging of atrial ablation procedures, ICE can be used for

FIGURE 4 Epicardial Fat



(A) Explanted heart of a patient with nonischemic cardiomyopathy who underwent cardiac transplantation after recurrent VT but for whom VT ablation procedures failed. The **white arrow** indicates the location of the AV groove. **(B)** 3D reconstruction of the color-coded epicardial fat tissue indicating the depth of the fat tissue. The **arrow** indicates the AV groove (shown in **A**); the thickness of the epicardial fat at this location is 15 mm. **(C)** 3D reconstruction of the epicardial fat thickness based on CT, indicating the fat thickness along the basal left ventricle. The **arrow** points to the AV groove (similar to panel shown in **A** and **B**), where the fat thickness is 15 mm. AV = atrioventricular; other abbreviations as in **Figures 1 and 2**.

FIGURE 5 Coronary Arteries and CT Angiography



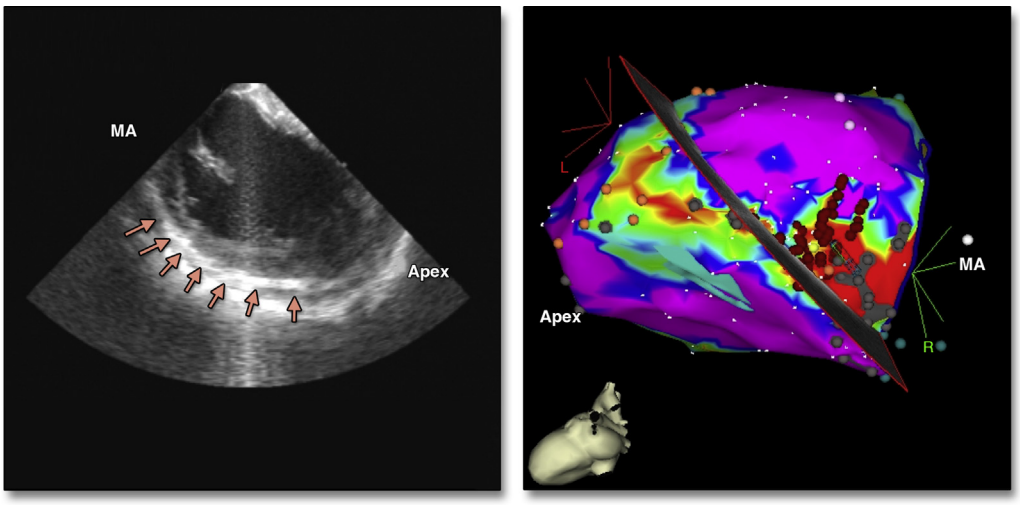
(Left) CT angiography of the left ventricle **(light green)**, the right ventricle **(dark green)**, and the aorta **(gray)** with the proximal left anterior descending (LAD) and diagonal arteries. Other coronary arteries are indicated. Electroanatomical map of the great cardiac vein and the anterior interventricular vein (mesh in **light blue color**) containing the mapping catheter positioned at the site of origin **(arrow)** of an epicardial VT. The phrenic nerve is shown in **yellow**. RAO **(top right)** and LAO **(bottom right)** views of coronary arteries. A **red circle** indicates the location of the ablation catheter adjacent to the LAD. No ablation was performed at the SOO, given the proximity to the coronary arteries. The VT was targeted from the adjacent right ventricle and was noninducible post ablation. CT images were processed using Music software (IHU Liryc, University of Bordeaux/Inria Sophia Antipolis). Cx = circumflex artery; LAO = left anterior oblique; RAO = right anterior oblique; RCA = right coronary artery; SOO = site of origin; VT = ventricular tachycardia; other abbreviation as in Figure 2.

ventricular ablation procedures. The CartoSound system uses real-time echocardiography data obtained through an ICE catheter (SoundStar, Biosense Webster) located in the right ventricle or right atrium. With this catheter, gated, 90°-sector image planes of the cardiac chamber of interest can be acquired and combined with a 3D CartoSound volume map. This real-time volume map can then be used for registration of CT or CMR images. The registration based on ICE data appears to be superior to the registration process using electroanatomical mapping data (68). The registration process is based on the best fit of both the echocardiographic 3D image reconstruction of CartoSound images and CT/CMR images.

As with the atrium, intracardiac thrombi can be detected in order to prevent thromboembolic events during mapping procedures. A study by Callans et al. (69) demonstrated that scar tissue can be identified by ICE in a porcine model. Infarcted myocardium can be identified by wall thinning and increased echodensity of the infarcted tissue (69). In patients with epicardial scar tissue, an increased echodensity of epicardial tissue seen on ICE has been correlated with scarring (70) (**Figure 6**).

The visual integration of the catheter tip (**Figure 7**) into the ultrasound image helps to correlate the real-time position of the catheter tip within the ultrasound image. This is of key importance to target arrhythmias from locations that are constantly moving, like the

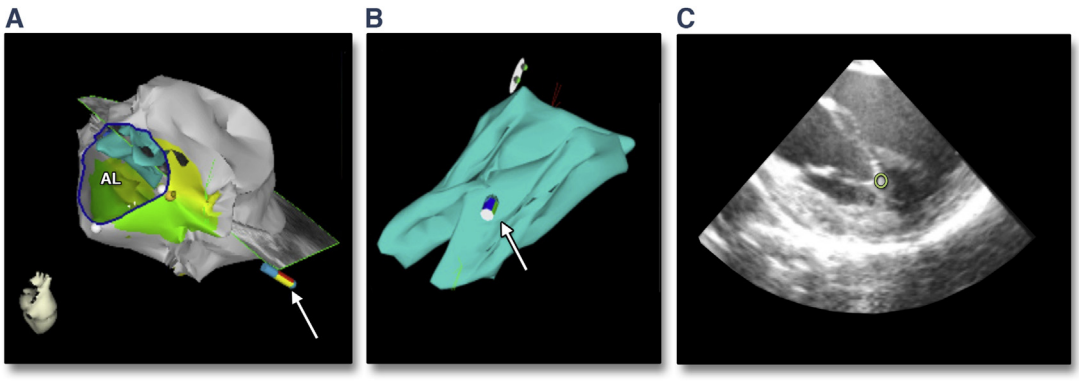
FIGURE 6 Epicardial Scarring and Intracardiac Echocardiography



(Left) 2D echocardiographic view of the left ventricle. The epicardial aspect of the posterolateral myocardium has higher echodensity **(arrows)** than the remainder of the myocardium. **(Right)** Electroanatomical bipolar epicardial voltage map with the location of the sector image plane displayed in the **left panel**. Increased echodensity **(left)** corresponds to an area of low voltage. MA = mitral valve annulus; 2D = 2-dimensional.

papillary muscles (71). Papillary muscle anatomy can be complex, and the challenge during the procedure is to investigate (map) the papillary muscles systematically to identify the origin of a ventricular arrhythmia and to keep the catheter at the site of origin while radiofrequency energy is delivered at a critical location (Figure 7). Constant monitoring of the catheter tip on the real-time echocardiogram is beneficial to achieve these objectives. When arrhythmias from the aortic cusps are targeted, the

FIGURE 7 Intracardiac Echocardiography and Papillary Muscles

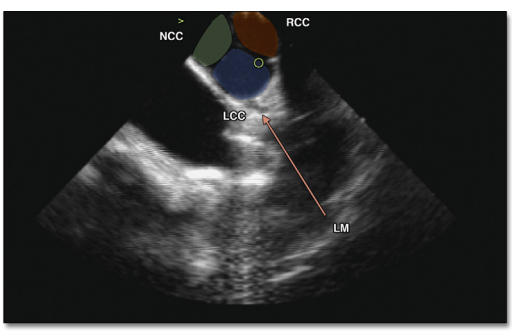


(A) 3D reconstruction of echocardiographic contours of the left ventricle. A single sector plane is shown originating from the tip of the echo probe **(white arrow)**. The mitral annulus is shown **(blue contour)**, and the anatomy of the anterolateral papillary muscle (AL) can be appreciated. **(B)** 3D reconstruction of the 2 heads of the anterolateral papillary muscle with the mapping/ablation catheter displayed on top of the papillary muscle bifurcation **(arrow)**. **(C)** Single 2D sector plane imaging the 2 heads of the anterolateral papillary muscle with the catheter in the bifurcation between the 2 heads of the papillary muscles. **Green circle** indicates the location of the tip of the ablation catheter in real time. Abbreviations as in Figures 2 and 6.

operator needs to make sure there is a safe distance between the location where radiofrequency energy is delivered and the origin of the coronary arteries. ICE enables the electrophysiologist to exactly locate the coronary ostia and mark this location on the electroanatomical map (Figure 8). Ablations have been carried out safely within a distance of >7 mm of the coronary arteries. When ablations are performed in the pulmonary arteries, the operator needs to be aware of the closer proximity to the left main coronary artery. Knowing whether the catheter is beyond the pulmonic valve (Figure 9), therefore, is helpful to avoid damage of the epicardial coronary arteries.

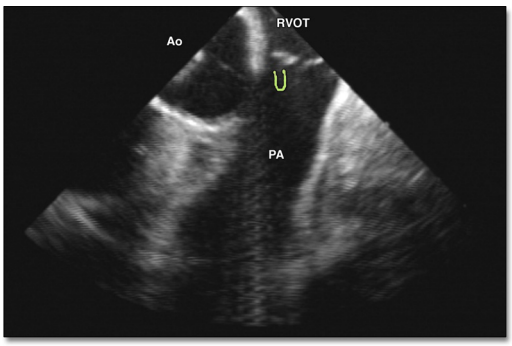
Real-time CMR-guided ablation procedures have been described in a few case series (72,73). This approach offers several theoretical advantages including the absence of ionizing radiation, the ability to image the entire myocardium in real time, the assessment of ablation lesions in real time, and the demonstration of scar tissue in real time and monitoring of temperature at the catheter-myocardial interface. The real-time CMR system is not approved by the U.S. Food and Drug Administration, however, and requires substantially changing the work-flow, including adaptation to a fundamentally different imaging modality that is unfamiliar to most electrophysiologists, and getting used to altered signals and electrocardiography in the CMR environment; furthermore, real-time CMR requires a substantial financial investment, as well as commitment from the electrophysiology staff (73).

FIGURE 8 ICE: Left Main Coronary Artery and Aortic Cusps With the Catheter in the LCC



The echocardiography probe is located in the right ventricular outflow tract and shows the aortic cusps: left coronary cusp (LCC) in **blue**; right coronary cusp (RCC) in **orange**; and noncoronary cusp (NCC) in **green**. The ostium of the left main (LM) coronary artery is shown with an **arrow**. The tip of the ablation catheter is shown with a **green** icon in the left coronary cusp. ICE = intracardiac echocardiography.

FIGURE 9 ICE: Ablation Catheter Beyond the Pulmonary Valve in the PA



The echocardiographic view of the aortic cusps (Ao) and the pulmonary artery (PA), while the echo probe is in the right ventricular outflow tract (RVOT) is shown. The ablation catheter **(green icon)** is beyond the pulmonary valve. In this patient, VT was ablated from within the pulmonary artery. ICE = intracardiac echocardiography; VT = ventricular tachycardia.

POST-PROCEDURE IMAGING

Just as after atrial fibrillation ablation procedures, CMRs can be performed to assess lesion formation (74). Unlike in cases of atrial fibrillation, this has not been used to assess long-term success of VT ablation procedures.

FUTURE ASPECTS AND STRATEGIES. Although progress has been made with respect to imaging of the arrhythmogenic substrate and integrating this information into mapping systems, there is still further room for improvement. Spatial resolution of scar imaging can be further improved and may help to better localize the arrhythmogenic substrate. Registration of image-related data is not perfect, and further progress in this is mandatory to avoid collateral damage if energy sources are used that are capable of generating large ablation lesions. Display of fiber orientation may also contain important information for arrhythmogenesis but imaging in vivo is problematic. Intracardiac echocardiography offers the advantages of real-time imaging and substrate identification; its role in identification of ablation lesions is investigational and will benefit from further development. Imaging has been found to reduce fluoroscopy exposure and procedure time. However, concerns about cost-effectiveness limits availability of certain imaging techniques, mainly because superior outcomes have not yet been demonstrated when imaging techniques have been used during ablation procedures.

CONCLUSIONS

Multimodality image integration into 3D electroanatomical mapping systems continues to change the landscape of ablation procedures in electrophysiology by lowering exposure to ionizing radiation and enhancing the safety of ablation procedures by providing information about cardiac anatomy and adjacent structures. Furthermore, imaging provides information about tissue integrity, and can thereby shorten procedure times and improve outcomes by focusing on areas of interest.

REPRINT REQUESTS AND CORRESPONDENCE: Dr. Frank Bogun, Cardiovascular Center, SPC 5853, 1500 East Medical Center Drive, Ann Arbor, Michigan 48109-5853. E-mail: fbogun@med.umich.edu.

REFERENCES

1. Pison L, Proclemer A, Bongiorni MG, et al. Imaging techniques in electrophysiology and implantable device procedures: results of the European Heart Rhythm Association survey. Europace 2013;15:1333–6.

2. Gepstein L, Hayam G, Ben-Haim SA. A novel method for nonfluoroscopic catheter-based electroanatomical mapping of the heart. In vitro and in vivo accuracy results. Circulation 1997;95:1611–22.

3. Gepstein L, Goldin A, Lessick J, et al. Electromechanical characterization of chronic myocardial infarction in the canine coronary occlusion model. Circulation 1998;98:2055–64.

4. Earley MJ, Showkathali R, Alzetani M, et al. Radiofrequency ablation of arrhythmias guided by non-fluoroscopic catheter location: a prospective randomized trial. Eur Heart J 2006;27:1223–9.

5. Scaglione M, Biasco L, Caponi D, et al. Visualization of multiple catheters with electroanatomical mapping reduces X-ray exposure during atrial fibrillation ablation. Europace 2011;13:955–62.

6. Stabile G, Scaglione M, del Greco M, et al. Reduced fluoroscopy exposure during ablation of atrial fibrillation using a novel electroanatomical navigation system: a multicentre experience. Europace 2012;14:60–5.

7. Heidbuchel H, Wittkampf FH, Vano E, et al. Practical ways to reduce radiation dose for patients and staff during device implantations and electrophysiological procedures. Europace 2014;16:946–64.

8. Finlay MC, Hunter RJ, Baker V, et al. A randomised comparison of Cartomerge vs. NavX fusion in the catheter ablation of atrial fibrillation: the CAVERN Trial. J Interv Card Electrophysiol 2012;33:161–9.

9. Cronin P, Kelly AM, Desjardins B, et al. Normative analysis of pulmonary vein drainage patterns on multidetector CT with measurements of pulmonary vein ostial diameter and distance to first bifurcation. Acad Radiol 2007;14:178–88.

10. Ang R, Hunter RJ, Baker V, et al. Pulmonary vein measurements on pre-procedural CT/MR imaging can predict difficult pulmonary vein isolation and phrenic nerve injury during cryoballoon ablation for paroxysmal atrial fibrillation. Int J Cardiol 2015;195:253–8.

11. Horton R, Di Biase L, Reddy V, et al. Locating the right phrenic nerve by imaging the right pericardiophrenic artery with computerized tomographic angiography: implications for balloon-based procedures. Heart Rhythm 2010;7:937–41.

12. Bertaglia E, Bella PD, Tondo C, et al. Image integration increases efficacy of paroxysmal atrial fibrillation catheter ablation: results from the CartoMerge Italian Registry. Europace 2009;11:1004–10.

13. Lemola K, Sneider M, Desjardins B, et al. Computed tomographic analysis of the anatomy of the left atrium and the esophagus: implications for left atrial catheter ablation. Circulation 2004;110:3655–60.

14. Good E, Oral H, Lemola K, et al. Movement of the esophagus during left atrial catheter ablation for atrial fibrillation. J Am Coll Cardiol 2005;46:2107–10.

15. Anter E, Silverstein J, Tschabrunn CM, et al. Comparison of intracardiac echocardiography and transesophageal echocardiography for imaging of the right and left atrial appendages. Heart Rhythm 2014;11:1890–7.

16. Patel A, Au E, Donegan K, et al. Multidetector row computed tomography for identification of left atrial appendage filling defects in patients undergoing pulmonary vein isolation for treatment of atrial fibrillation: comparison with transesophageal echocardiography. Heart Rhythm 2008;5:253–60.

17. Rathi VK, Reddy ST, Anreddy S, et al. Contrast-enhanced CMR is equally effective as TEE in the evaluation of left atrial appendage thrombus in patients with atrial fibrillation undergoing pulmonary vein isolation procedure. Heart Rhythm 2013;10:1021–7.

18. Parikh SS, Jons C, McNitt S, Daubert JP, Schwarz KQ, Hall B. Predictive capability of left atrial size measured by CT, TEE, and TTE for recurrence of atrial fibrillation following radiofrequency catheter ablation. Pacing Clin Electrophysiol 2010;33:532–40.

19. Oakes RS, Badger TJ, Kholmovski EG, et al. Detection and quantification of left atrial structural remodeling with delayed-enhancement magnetic resonance imaging in patients with atrial fibrillation. Circulation 2009;119:1758–67.

20. Mahnkopf C, Badger TJ, Burgon NS, et al. Evaluation of the left atrial substrate in patients with lone atrial fibrillation using delayed-enhanced MRI: implications for disease progression and response to catheter ablation. Heart Rhythm 2010;7:1475–81.

21. Cummings JE, Schweikert R, Saliba W, et al. Left atrial flutter following pulmonary vein antrum isolation with radiofrequency energy: linear lesions or repeat isolation. J Cardiovasc Electrophysiol 2005;16:293–7.

22. Dravid SG, Hope B, McKinnie JJ. Intracardiac echocardiography in electrophysiology: a review of current applications in practice. Echocardiography 2008;25:1172–5.

23. Peters DC, Wylie JV, Hauser TH, et al. Detection of pulmonary vein and left atrial scar after catheter ablation with three-dimensional navigator-gated delayed enhancement MR imaging: initial experience. Radiology 2007;243:690–5.

24. Kapa S, Desjardins B, Callans DJ, Marchlinski FE, Dixit S. Contact electroanatomical mapping derived voltage criteria for characterizing left atrial scar in patients undergoing ablation for atrial fibrillation. J Cardiovasc Electrophysiol 2014;25:1044–52.

25. McGann CJ, Kholmovski EG, Oakes RS, et al. New magnetic resonance imaging-based method for defining the extent of left atrial wall injury after the ablation of atrial fibrillation. J Am Coll Cardiol 2008;52:1263–71.

26. Reddy VY, Shah D, Kautzner J, et al. The relationship between contact force and clinical outcome during radiofrequency catheter ablation of atrial fibrillation in the TOCCATA study. Heart Rhythm 2012;9:1789–95.

27. Akca F, Janse P, Theuns DA, Szili-Torok T. A prospective study on safety of catheter ablation procedures: contact force guided ablation could reduce the risk of cardiac perforation. Int J Cardiol 2015;179:441–8.

28. Dickfeld T, Kato R, Zviman M, et al. Characterization of radiofrequency ablation lesions with gadolinium-enhanced cardiovascular magnetic resonance imaging. J Am Coll Cardiol 2006;47:370–8.

29. Kim RJ, Fieno DS, Parrish TB, et al. Relationship of MRI delayed contrast enhancement to irreversible injury, infarct age, and contractile function. Circulation 1999;100:1992–2002.

30. Ranjan R, Kholmovski E, Silvernagel J, Vijayakumar S, Marrouche N. Acute assessment of radiofrequency ablation lesions in MRI without the use of gadolinium based contrast. J Am Coll Cardiol 2014;63 Supp A:A94.

31. Badger TJ, Daccarett M, Akoum NW, et al. Evaluation of left atrial lesions after initial and repeat atrial fibrillation ablation: lessons learned from delayed-enhancement MRI in repeat ablation procedures. Circ Arrhythm Electrophysiol 2010;3:249–59.

32. Ranjan R, Kato R, Zviman MM, et al. Gaps in the ablation line as a potential cause of recovery from electrical isolation and their visualization using MRI. Circ Arrhythm Electrophysiol 2011;4:279–86.

33. Eyerly SA, Bahnson TD, Koontz JI, et al. Intracardiac acoustic radiation force impulse imaging: a novel imaging method for intraprocedural evaluation of radiofrequency ablation lesions. Heart Rhythm 2012;9:1855–62.

34. Marchlinski FE, Callans DJ, Gottlieb CD, Zado E. Linear ablation lesions for control of unmappable ventricular tachycardia in patients with ischemic and nonischemic cardiomyopathy. Circulation 2000;101:1288–96.

35. Perin EC, Silva GV, Sarmento-Leite R, et al. Assessing myocardial viability and infarct transmurality with left ventricular electromechanical mapping in patients with stable coronary artery disease: validation by delayed enhancement magnetic resonance imaging. Circulation 2002;106:957–61.

36. Desjardins B, Crawford T, Good E, et al. Infarct architecture and characteristics on delayed enhanced magnetic resonance imaging and electroanatomical mapping in patients with post-infarction ventricular arrhythmia. Heart Rhythm 2009;6:644–51.

37. Codreanu A, Odille F, Aliot E, et al. Electroanatomic characterization of post-infarct scars comparison with 3-dimensional myocardial scar reconstruction based on magnetic resonance imaging. J Am Coll Cardiol 2008;52:839–42.

38. Bogun FM, Desjardins B, Good E, et al. Delayed-enhanced magnetic resonance imaging in nonischemic cardiomyopathy: utility for identifying the ventricular arrhythmia substrate. J Am Coll Cardiol 2009;53:1138–45.

39. Kim RJ, Chen EL, Lima JA, Judd RM. Myocardial Gd-DTPA kinetics determine MRI contrast enhancement and reflect the extent and severity of myocardial injury after acute reperfused infarction. Circulation 1996;94:3318–26.

40. Njeim M, Yokokawa M, Frank L, et al. Value of cardiac magnetic resonance imaging in patients with failed ablation procedures for ventricular tachycardia. J Cardiovasc Electrophysiol 2016;27:183–9.

41. Mueller G, Bogun F. Role of MRI in Mapping of the Architecture of Arrhythmia Substrate in Patients with Ischemic and Non-ischemic Cardiomyopathy. Cardiac Mapping. 4th edition. Hoboken, NJ: Wiley-Blackwell, 2012.

42. Gupta S, Desjardins B, Baman T, et al. Delayed-enhanced MR scar imaging and intraprocedural registration into an electroanatomical mapping system in post-infarction patients. J Am Coll Cardiol Img 2012;5:207–10.

43. Perez-David E, Arenal A, Rubio-Guivernau JL, et al. Noninvasive identification of ventricular tachycardia-related conducting channels using contrast-enhanced magnetic resonance imaging in patients with chronic myocardial infarction: comparison of signal intensity scar mapping and endocardial voltage mapping. J Am Coll Cardiol 2011;57:184–94.

44. Komatsu Y, Cochet H, Jadidi A, et al. Regional myocardial wall thinning at multidetector computed tomography correlates to arrhythmogenic substrate in postinfarction ventricular tachycardia: assessment of structural and electrical substrate. Circ Arrhythm Electrophysiol 2013;6:342–50.

45. Hutchinson MD, Gerstenfeld EP, Desjardins B, et al. Endocardial unipolar voltage mapping to detect epicardial ventricular tachycardia substrate in patients with nonischemic left ventricular cardiomyopathy. Circ Arrhythm Electrophysiol 2011;4:49–55.

46. Desjardins B, Yokokawa M, Good E, et al. Characteristics of intramural scar in patients with nonischemic cardiomyopathy and relation to intramural ventricular arrhythmias. Circ Arrhythm Electrophysiol 2013;6:891–7.

47. Sasano T, Abraham MR, Chang KC, et al. Abnormal sympathetic innervation of viable myocardium and the substrate of ventricular tachycardia after myocardial infarction. J Am Coll Cardiol 2008;51:2266–75.

48. Fallavollita JA, Heavey BM, Luisi AJ Jr., et al. Regional myocardial sympathetic denervation predicts the risk of sudden cardiac arrest in ischemic cardiomyopathy. J Am Coll Cardiol 2014;63:141–9.

49. Kammerling JJ, Green FJ, Watanabe AM, et al. Denervation supersensitivity of refractoriness in noninfarcted areas apical to transmural myocardial infarction. Circulation 1987;76:383–93.

50. Simoes MV, Barthel P, Matsunari I, et al. Presence of sympathetically denervated but viable myocardium and its electrophysiologic correlates after early revascularised, acute myocardial infarction. Eur Heart J 2004;25:551–7.

51. Klein T, Abdulghani M, Smith M, et al. Three-dimensional 123I-meta-iodobenzylguanidine cardiac innervation maps to assess substrate and successful ablation sites for ventricular tachycardia: feasibility study for a novel paradigm of innervation imaging. Circ Arrhythm Electrophysiol 2015;8:583–91.

52. Wollenweber T, Bengel FM. Molecular imaging to predict ventricular arrhythmia in heart failure. J Nucl Cardiol 2014;21:1096–109.

53. Neilan TG, Coelho-Filho OR, Danik SB, et al. CMR quantification of myocardial scar provides additive prognostic information in nonischemic cardiomyopathy. J Am Coll Cardiol Img 2013;6:944–54.

54. Sosa E, Scanavacca M, d'Avila A, Pilleggi F. A new technique to perform epicardial mapping in the electrophysiology laboratory. J Cardiovasc Electrophysiol 1996;7:531–6.

55. Marcus FI, McKenna WJ, Sherrill D, et al. Diagnosis of arrhythmogenic right ventricular cardiomyopathy/dysplasia: proposed modification of the task force criteria. Circulation 2010;121:1533–41.

56. Komatsu Y, Jadidi A, Sacher F, et al. Relationship between MDCT-imaged myocardial fat and ventricular tachycardia substrate in arrhythmogenic right ventricular cardiomyopathy. J Am Heart Assoc 2014;3:e000935.

57. Santangeli P, Di Biase L, Lakkireddy D, et al. Radiofrequency catheter ablation of ventricular arrhythmias in patients with hypertrophic cardiomyopathy: safety and feasibility. Heart Rhythm 2010;7:1036–42.

58. Dukkipati SR, d'Avila A, Soejima K, et al. Long-term outcomes of combined epicardial and endocardial ablation of monomorphic ventricular tachycardia related to hypertrophic cardiomyopathy. Circ Arrhythm Electrophysiol 2011;4:185–94.

59. Desjardins B, Morady F, Bogun F. Effect of epicardial fat on electroanatomical mapping and epicardial catheter ablation. J Am Coll Cardiol 2010;56:1320–7.

60. Carrigan TP, Patel S, Yokokawa M, et al. Anatomic relationships between the coronary venous system, surrounding structures, and the site of origin of epicardial ventricular arrhythmias. J Cardiovasc Electrophysiol 2014;25:1336–42.

61. Santangeli P, Marchlinski FE, Zado ES, et al. Percutaneous epicardial ablation of ventricular arrhythmias arising from the left ventricular summit: outcomes and electrocardiogram correlates of success. Circ Arrhythm Electrophysiol 2015;8:337–43.

62. Yokokawa M, Latchamsetty R, Good E, et al. Ablation of epicardial ventricular arrhythmias from nonepicardial sites. Heart Rhythm 2011;8:1525–9.

63. Baman TS, Ilg KJ, Gupta SK, et al. Mapping and ablation of epicardial idiopathic ventricular arrhythmias from within the coronary venous system. Circ Arrhythm Electrophysiol 2010;3:274–9.

64. D'Avila A, Gutierrez P, Scanavacca M, et al. Effects of radiofrequency pulses delivered in the vicinity of the coronary arteries: implications for nonsurgical transthoracic epicardial catheter ablation to treat ventricular tachycardia. Pacing Clin Electrophysiol 2002;25:1488–95.

65. Yamashita S, Sacher F, Mahida S, et al. Role of high-resolution image integration to visualize left phrenic nerve and coronary arteries during epicardial ventricular tachycardia ablation. Circ Arrhythm Electrophysiol 2015;8:371–80.

66. Buch E, Vaseghi M, Cesario DA, Shivkumar K. A novel method for preventing phrenic nerve injury during catheter ablation. Heart Rhythm 2007;4:95–8.

67. Di Biase L, Burkhardt JD, Pelargonio G, et al. Prevention of phrenic nerve injury during epicardial ablation: comparison of methods for separating the phrenic nerve from the epicardial surface. Heart Rhythm 2009;6:957–61.

68. Bunch TJ, Weiss JP, Crandall BG, et al. Image integration using intracardiac ultrasound and 3D reconstruction for scar mapping and ablation of ventricular tachycardia. J Cardiovasc Electrophysiol 2010;21:678–84.

69. Callans DJ, Ren JF, Michele J, Marchlinski FE, Dillon SM. Electroanatomic left ventricular mapping in the porcine model of healed anterior

myocardial infarction. Correlation with intracardiac echocardiography and pathological analysis. Circulation 1999;100:1744–50.

70. Bala R, Ren JF, Hutchinson MD, et al. Assessing epicardial substrate using intracardiac echocardiography during VT ablation. Circ Arrhythm Electrophysiol 2011;4:667–73.

71. Good E, Desjardins B, Jongnarangsin K, et al. Ventricular arrhythmias originating from a papillary muscle in patients without prior infarction: a comparison with fascicular arrhythmias. Heart Rhythm 2008;5:1530–7.

72. Eitel C, Piorkowski C, Hindricks G, Gutberlet M. Electrophysiology study guided by real-time magnetic resonance imaging. Eur Heart J 2012;33:1975.

73. Piorkowski C, Grothoff M, Gaspar T, et al. Cavotricuspid isthmus ablation guided by real-time magnetic resonance imaging. Circ Arrhythm Electrophysiol 2013;6:e7–10.

74. Ilg K, Baman TS, Gupta SK, et al. Assessment of radiofrequency ablation lesions by CMR imaging after ablation of idiopathic ventricular arrhythmias. J Am Coll Cardiol Img 2010;3:278–85.

75. Caponi D, Corleto A, Scaglione M, et al. Ablation of atrial fibrillation: does the addition of three-dimensional magnetic resonance imaging of the left atrium to electroanatomical mapping improve the clinical outcome? A randomized comparison of Carto-Merge vs. Carto-XP three-dimensional mapping ablation in patients with paroxysmal and persistent atrial fibrillation. Europace 2010;12:1098–104.

76. Brooks AG, Wilson L, Chia NH, et al. Accuracy and clinical outcomes of CT image integration with Carto-Sound compared to electro-anatomical mapping for atrial fibrillation ablation: a randomized controlled study. Int J Cardiol 2013;168:2774–82.

77. Tang K, Ma J, Zhang S, et al. A randomized prospective comparison of CartoMerge and CartoXP to guide circumferential pulmonary vein isolation for the treatment of paroxysmal atrial fibrillation. Chin Med J (Engl) 2008;121:508–12.

78. Lamberti F, Di Clemente F, Remoli R, et al. Catheter ablation of idiopathic ventricular tachycardia without the use of fluoroscopy. Int J Cardiol 2015;190:338–43.

KEY WORDS ablation, atrial fibrillation, multimodality imaging, ventricular tachycardia